Journal of Physics: Conference Series **1623** (2020) 012009 doi:10.1088/1742-6596/1623/1/012009

Galactic cosmic ray propagation models using Picard

R. Kissmann[1], J. Thaler[1], O. Reimer[1]

[1]Institut für Astro- und Teilchenphysik, Leopold-Franzens Universität Innsbruck

E-mail: ralf.kissmann@uibk.ac.at

Abstract. We will give an overview of recent developments in numerical modelling of CR transport in our Galaxy with the Picard code. Corresponding numerical models aim at reproducing CR spectra and also diffuse gamma-ray emission from the Galaxy by solving the cosmic-ray transport problem in a three-dimensional model of the Galaxy. We address the impact of different transport physics processes on the flux and distribution of diffuse Galactic gamma rays: we investigate CR transport using different cosmic-ray source distribution models ranging from smooth source distributions to localised sources related to high-energy gamma-ray observations. Additionally, we consider anisotropic cosmic-ray diffusion in an improved Galactic magnetic field model. The choice of changing the different transport parameters is most readily visible in the inverse-Compton channel, which shows features not present in commonly-used axisymmetric transport models.

1. Introduction

Research on cosmic rays started more than 100 years ago, with the detection of ionising radiation from outer space. Since then they have been thoroughly studied by experiments and analytical and numerical modelling. Here, we focus on recent advancements of the modelling efforts for Galactic cosmic-rays, i.e. those cosmic rays for which the sources are located within our Galaxy, in the context of the Picard code. Detection of the cosmic-ray flux at Earth yields their local spectrum but only little information on their distribution throughout or on their origin within our Galaxy. While an analysis of their isotopic abundance gives some ideas about their traversed gas mass within the Galaxy, only secondary messengers like electromagnetic radiation (synchrotron or gamma-ray emission) or neutrinos can safely indicate directions in which the density of cosmic rays is high within our Galaxy. Since these photons and neutrinos originate from interactions of the cosmic rays with some target field (interstellar magnetic field, interstellar radiation field, or interstellar matter), determining the distribution of cosmic rays from such observations can not directly be done, especially since observations of photons and neutrinos only give directional information but no answer on the distance, where the photons or neutrinos have been produced.

The usual approach, therefore, is to build a model for the spatial distribution of cosmic-rays within our Galaxy and compute the corresponding Galactic diffuse gamma-ray or neutrino emission. By identifying the differences between these model results and observations, the relevant deviations can be identified and the models are modified accordingly. This process relies on the one hand on an accurate model for the transport of cosmic rays within the Galaxy and on the other hand on an accurate model for the different target fields within our Galaxy. Since the cosmic-rays are also affected by these target fields, their distribution is also relevant for the transport model. Correspondingly, recent efforts to improve Galactic cosmic-ray transport

modelling partly focus on a better description of the matter density within the Galaxy (see, e.g.,(1; 2; 3; 4; 5; 6; 7)).

Cosmic-ray transport can be mathematically described via the transport equation:

$$\frac{\partial \psi_i}{\partial t} = q(\vec{r},p) + \nabla\cdot\mathcal{D}\nabla\psi_i + \frac{\partial}{\partial p}p^2 D_{pp}\frac{\partial}{\partial p}\frac{1}{p^2}\psi_i - \nabla\cdot\vec{v}\psi_i - \frac{\partial}{\partial p}\left\{\dot{p}\psi_i - \frac{p}{3}(\nabla\cdot\vec{v})\psi_i\right\} - \frac{1}{\tau_f}\psi_i - \frac{1}{\tau_r}\psi_i. \quad (1)$$

where ψ_i is the density of species i per unit of momentum p; $q(\vec{r},p)$ describes the distribution of source in space together with their momentum dependence also including sources from spallation or decay of other cosmic-ray species; $\mathcal{D}$ is the spatial diffusion tensor; $\vec{v}$ is the convection velocity; D_{pp} is the energy-dependent coefficient determining diffusive reacceleration; $\dot{p}$ represents momentum gains or losses, and τ_f and τ_r represent timescales for fundamental losses by fragmentation and radioactive decay, respectively. As seen in the previous discussion, a change in the model of the Galactic matter distribution also affects the cosmic-ray source term $q(\vec{r},p)$ (including the spallation term from other cosmic-ray species), their energy losses, and also the spatial dependence of τ_f. Since we do not have an accurate model for the matter distribution within our Galaxy available, there is a huge variety in the resulting models to be expected.

Apart from that, some parameters of the cosmic-ray transport equation are not accurately known: cross-sections for fragmentation rely on sparse measurements (see, e.g., (8; 9)) usually taken at much lower energies. Also, fundamental theories for cosmic-ray transport (10; 11; 12; 13; 14) cannot be easily applied, considering that the magnetic field strength and turbulence conditions in the interstellar medium are only loosely constrained. Correspondingly, there is a range of studies that try to determine these transport parameters either from statistical fits (15; 16) or from fits to observables related to cosmic rays (17; 18).

Within the context of simulations using the PICARD code, we focussed on adapting the Galactic matter distribution via consideration of a new radiation field (19; 5) and more complex distributions of primary cosmic-ray sources (7; 4). Additionally, we considered more complex transport physics, where we investigated the effects of anisotropic spatial diffusion, in contrast to the majority of Galactic cosmic-ray transport models that rely on isotropic diffusion. Apart from such adaptions of the transport physics, with PICARD we also try to improve the numerical solution methods for Galactic cosmic-ray transport. For this we are currently testing different numerical solvers for linear systems of equations. At the same time, PICARD has a close control of the numerical error, with the different sub solvers having been subject to a range of different tests (20). In the following Sec. 2, we will discuss some peculiarities of the axisymmetric scheme in PICARD and show the relevance of the numerical error control. Then, we will discuss some recent applications of PICARD in Sec. 3. Finally, we end with a short conclusion.

2. Numerical Scheme

The scientific literature provides a range of different numerical approaches to solve the cosmic-ray transport problem, depending on the focus of the related application. For approximate studies of the cosmic-ray flux at Earth or large-scale parameter studies often semi-analytical approaches are used that allow a fast solution for a simplified model of the Galaxy. This is, e.g., realized in the context of the publicly available code USINE (21). Whenever emission of gamma-rays or other secondaries is of interest a more complex model of the Galaxy becomes necessary, which also requires the use of a fully numerical solutions method. Also for this, there are different approaches available. Codes like PICARD, DRAGON (22), or GALPROP (23; 24) solve the transport equation on a grid in space and energy, where in principal arbitrary models can be used for the Galaxy.

As an alternative to such grid-based approaches different groups solve the transport problem either by investigating the propagation of a large statistical sample of individual particles (see,

e.g., (25)) or by using a stochastic-differential-equation approach, where the propagation of phase-space density elements is followed in time (26; 27; 28). Especially the latter approach is very efficient, when investigating the cosmic-ray flux at individual locations, but becomes numerically expensive, when investigating, e.g, the emission of gamma rays, where the cosmic-ray flux needs to be computed everywhere in the Galaxy.

Therefore, in the following we focus on grid-based codes, where we will only discuss steady-state problems. In that case, DRAGON and GALPROP use a similar numerical scheme to solve the cosmic-ray transport equation: the transport equation is integrated in time until presumably a steady-state solution is found (see the discussion in appendix B of (24)). In contrast, PICARD directly solves the steady-state problem, leading to an efficient solution scheme with a direct control of the numerical error, as extensively discussed in (20). For the solution of steady-state problems, PICARD provides a plain-diffusion scheme, that is only applicable without reacceleration and other energy gains, and a full scheme that can be applied to the full steady-state transport equation. In the following, we will focus on the latter scheme. While PICARD was developed to efficiently solve spatially three-dimensional problems, recently also an analogous solver for axisymmetric problems, as they are often used in Galactic cosmic-ray transport modelling (29; 17), has been implemented.

2.1. Axisymmetric Solver

This scheme uses the same basic approach to solve the cosmic-ray transport problem as the three-dimensional scheme, i.e. a discretisation of the steady-state transport equation together with a multigrid solver for the resulting linear system of equations. However, the use of cylindrical coordinates requires a special treatment of the radial grid to allow a consistent treatment of the grid singularity in the radial dimension. The multigrid method (see (30)) is an iterative scheme, where the problem is mapped from the standard grid to successively coarser grids, on which the error on large scales converges more efficiently. For the axisymmetric solver this leads to the additional problem, that a treatment of the singularity in the radial dimension becomes necessary on each grid level. This means in particular that the grid needs to be designed in a way that the discrete spatial diffusion operator can work with meaningful quantities at all gridpoints.

The spatial diffusion operator for the axisymmetric case reads:

$$\nabla \cdot \mathcal{D}\nabla\psi = (\nabla \cdot \mathcal{D}\nabla\psi)_{rr} + (\nabla \cdot \mathcal{D}\nabla\psi)_{zz} \tag{2}$$

with

$$(\nabla \cdot \mathcal{D}\nabla\psi)_{rr} = \frac{1}{r}\frac{\partial}{\partial r}\left(rD_{rr}\frac{\partial\psi}{\partial r}\right) \quad \text{and} \quad (\nabla \cdot \mathcal{D}\nabla\psi)_{zz} = \frac{\partial}{\partial z}\left(D_{zz}\frac{\partial\psi}{\partial z}\right) \tag{3}$$

where we assumed the diffusion tensor to be diagonal, in this case. In PICARD we use the following discrete form of this operator:

$$(\nabla \cdot \mathcal{D}\nabla\psi)^{\text{disc}}_{rr} = \frac{1}{r_i\Delta r_i}\left(D_{rr;i+1/2}r_{i+1/2}\frac{\psi_{i+1}-\psi_i}{\Delta r_{i+1/2}} - D_{rr;i-1/2}r_{i-1/2}\frac{\psi_i-\psi_{i-1}}{\Delta r_{i-1/2}}\right) \tag{4}$$

Here, the index i indicates the cell C_i under consideration and half-integral indices refer to the boundaries between cells. Evaluating this expression at the origin leads to problems due to presence of the $1/r_i$ term. Therefore, we used a cell-wise discretisation of the radial grid with the radially innermost cell C_0 ranging from 0 to Δr, i.e., we have $r_0 = \Delta r/2$. By this, we made sure that the $1/r_i$ factor cannot cause problems for the innermost cell and also the second term in the brackets in Eq. (4) is identical to zero, there. If ghost-cell values at $i = -1$ should be necessary, we use $\psi_{-1} = \psi_0$, which follows from the axisymmetry of the problem.

So far, we only addressed the construction of the grid on the finest level of the multigrid hierarchy, i.e., on the level, for which we specify our transport problem. In the other spatial dimensions, including all dimensions of a three-dimensional Cartesian setup, a coarse grid is constructed from a finer grid as follows: for a fine grid with grid points $j_f = 0 \dots 2^{n_f}$ in a given direction we obtain a coarse grid as $j_c = 0 \dots 2^{n_c}$, where $n_c = n_f/2$. In this case, the coarse grid only has grid points at the location of the even grid points of the fine grid. That also means that on the coarse grid the spacing of the grid points is twice the spacing on the fine grid. This grid construction is not suitable for the radial coordinate in the axisymmetric case, because the position $r_{i-1/2}$ of cell C_0 would not coincide with the origin anymore.

This issue is solved by using a cell-wise instead of a point-wise discretisation of the grid. In this case we use $N_f = 2^{n_f}$ cells on the finest grid, where, for a linear grid, the cell centres are located at:

$$r_i^f = \Delta_r^f/2 + i\Delta_r^f \qquad \text{with} \qquad i = 0 \dots N_f - 1 \tag{5}$$

Thus, the innermost cell ranges from $r^f_{-1/2} = 0$ to $r^f_{1/2} = \Delta^f_r$. In this case, the coarse grid is constructed by joining two adjacent grid cells into a new grid cell with twice the radial extent. Correspondingly, we have $N_c = 2^{n_c}$ with $n_c = n_f/2$ and $\Delta^c_r = 2\Delta^f_r$. This also means that the innermost cell on the coarse grid extends from $r^c_{-1/2} = 0$ to $r^c_{1/2} = \Delta^c_r$. By this construction the center of the innermost cell is one half cell width away from the origin on all coarse grids. As a result also the discretisation of the radial part of the diffusion term is of the same form for the innermost radial cell on all grid levels and no problems by the singularity occur. This different grid construction also required implementation of different transfer operators between the different multigrid levels, for which standard transfer operators as discussed in (31) were used. In the following we will briefly apply this specific scheme to discuss the accuracy of the solver within PICARD.

2.2. Accuracy of the Solver

When introducing a new code, e.g., on the field of astrophysical fluid dynamics, it is mandatory to verify the capability of the code via a suite of standard tests and discuss convergence properties of the code. Interestingly, such studies are highly unusual in Galactic cosmic-ray transport modelling. Reasons for this might be the comparatively simple numerical solver together with the limited number of solvers publicly available. Here, we argue that an entire code modelling cosmic-ray transport for a full nuclear network is sufficiently complex to warrant extensive testing and comparison to other implementations. Some corresponding numerical tests are discussed in (20). Apart from that the convergence properties are monitored in each PICARD simulation, where a steady-state result is extracted, only when the residual is below a specified bound. For this the transport equation is rewritten as:

$$\mathcal{L}\psi_i = q(\vec{r}, p) \tag{6}$$

where $\mathcal{L}$ is the differential operator from Eq. (1). By discretising this differential operator we end up with a linear system of equations of the form

$$\hat{L}\vec{\psi_i} = \vec{q} \tag{7}$$

where $\hat{L}$ is the matrix of the linear system of equations, coupling the point values $\vec{\psi_i}$ at each grid point, with $\vec{q}$ the vector of source terms at each point. From this, the residual is computed via:

$$\vec{r} = \vec{q} - \hat{L}\vec{\psi_i} \tag{8}$$

Usually, we require the l2 and the l∞ norms of the relative residual to be below $\epsilon \sim 10^{-5}$. For this value, we can be sure that the iterations of the multigrid scheme are sufficiently converged

for the error of the scheme to be much smaller than the actual discretisation error. This can, e.g., be seen by comparing results for different tolerances on the relative residual as shown in Fig. 1. There we show simulation results using the axisymmetric solver discussed in Sec. 2.1 for antiprotons. Apparently, there are no relevant differences for solutions with $\epsilon < 0.001$ anymore, so using $\epsilon \sim 10^{-5}$ is actually a very conservative choice.

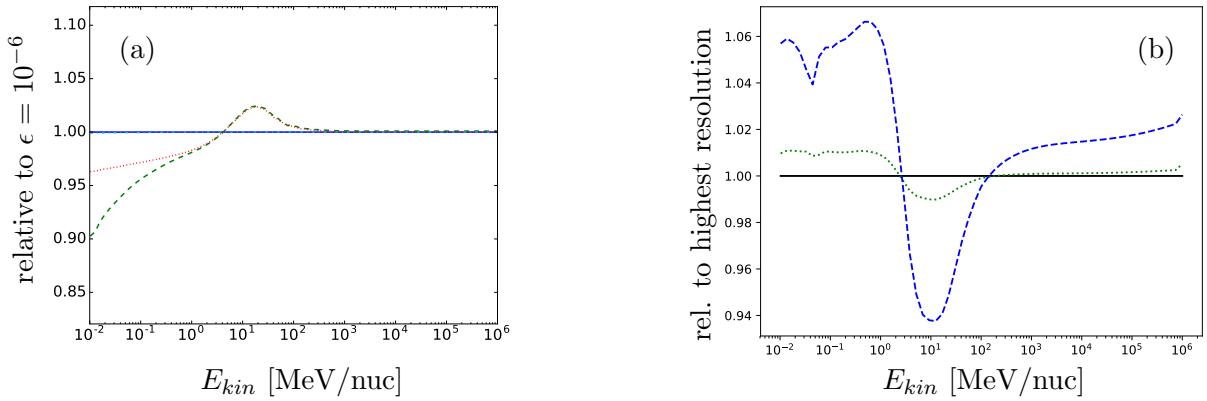

Figure 1. (a) Relative deviations of the $\bar{p}$ cosmic-ray flux for different stopping criteria for the multigrid iterations. Here we compare solutions for $\epsilon = 0.1$ (green dashed), $\epsilon = 0.01$ (red dotted), and $\epsilon = 0.001$ (cyan dash-dotted) with those for $\epsilon = 10^{-6}$. (b) Relative deviations of the ^{10}B cosmic-ray flux for different resolutions. Here we compare $N_r = 64, N_z = 33, N_p = 63$ (blue dashed) and $N_r = 128, N_z = 65, N_p = 127$ (green dotted) with a high-resolution model with $N_r = 256, N_z = 129, N_p = 255$.

So far, this only gives a hint about the convergence property of the multigrid solver, but we can not infer expected absolute error values that can still originate from the discretisation in space and momentum. Therefore, we did a further study, also using the axisymmetric solver, where we compared results for different resolutions in space and momentum. In this case, we investigated the flux of ^{10}B for different resolutions, where Fig. 1 shows the deviations from a high-resolution simulation. Apparently, we find deviations on the one-percent level at a resolution of $N_r = 128, N_z = 65, N_p = 127$, which is rather typical for axisymmetric Galactic cosmic-ray modelling. In the future, it will be interesting to compare to the performance of other codes like, e.g., Galprop (23; 24), because at least in some versions of Galprop the discretisation of the momentum losses is of first order. In Picard we use a second-order finite-difference discretisation in order to avoid poor performance from the discretisation of momentum derivatives (see also the discussion in (22)). This discussion shows on the one hand that errors for results produced with Picard are comparatively well-constrained, and on the other hand that a more thorough discussion and testing of cosmic-ray propagation codes is worthwhile.

3. Developments in Transport Physics

Typical applications of the Picard code focus on its capability to efficiently solver three-dimensional transport problems. The prime example in this case is the investigation of the impact of different three-dimensional cosmic-ray source distributions, discussed in (7; 4). There, we focused on different analytically-prescribed source distributions from axisymmetric configurations to different spiral-arm source distributions.

In (4) we started from an established axisymmetric base model adapted from (32), where we modified the transport parameters for the spiral-arm source distributions models in a way

that we find a good fit of the cosmic-ray spectra at Earth. For this, we only changed the spatial diffusion coefficient and the coefficient for diffusive re-acceleration via the Alfvén speed, assumed to be constant throughout the numerical domain. All other parameters were used as given by model ${}^{\mathrm{S}}\mathrm{Y}^{\mathrm{Z}}4^{\mathrm{R}}20^{\mathrm{T}}150^{\mathrm{C}}5$ from (32). For solving the transport problem, we used the same axisymmetric model for the gas distribution, which is extensively discussed in (33).

Since the spatial structure of the gas is especially relevant for the computation of the ensuing gamma-ray emission, we again use the same setup as (32), where from observations of the different gas phases column-density maps for a range of Galactocentric annuli were computed. Only recently, there have been some efforts to investigate alternative gas models for the Galaxy and quantify the impact on gamma-ray emission (3) (see also (1) for a similar study relating to the Galactic center). Currently, there are also further efforts regarding the computation of gamma-ray emission for Galactic cosmic-ray transport models (34), where also alternative gas-distribution models are investigated.

In (4) we showed that we can find a good fit to observed cosmic-ray spectra at Earth both for the axisymmetric base model and also for a spiral-arm source distribution model following the parametrization by (35). The distribution of cosmic-rays in the Galaxy for both models is of course rather different. As a result also the ensuing gamma-ray emission is different in both models as shown in Fig. 2 (and also discussed in (36)).

Due to the excessive energy losses of high-energy electrons they only occur in the close vicinity of their sources. Correspondingly, the imprint of different source models becomes mostly apparent in the inverse-Compton gamma-ray emission. This is readily visible from Fig. 2, via the imprint of the spiral-arm tangents as opposed to the more homogeneous emission for a model using an axisymmetric source distribution.

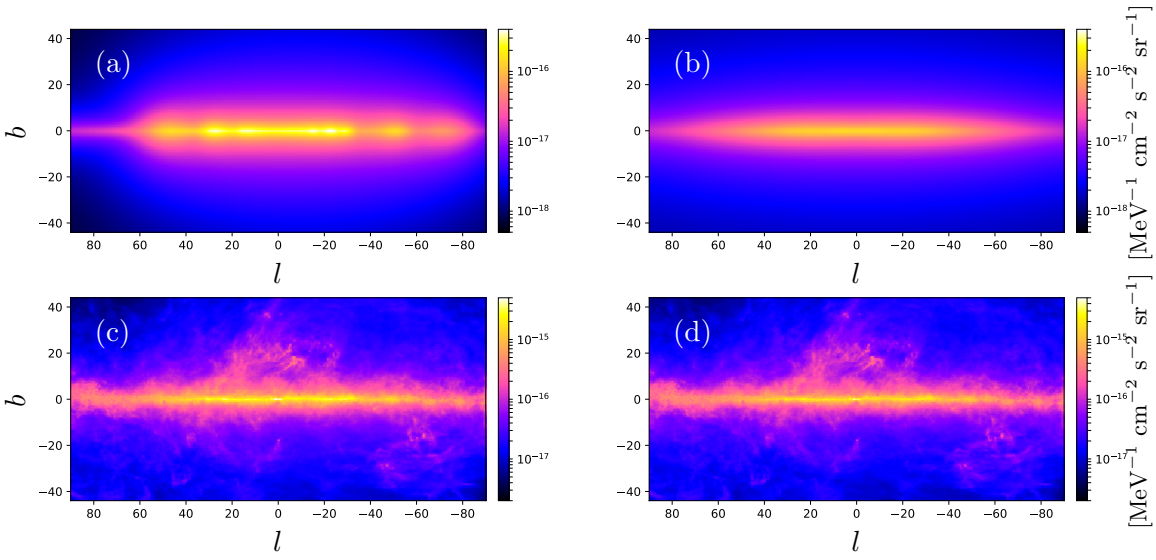

Figure 2. Inverse-Compton gamma-ray emission (top; images (a) and (b)) and total gamma-ray emission (bottom; images(c) and (d)) at ∼1 TeV for the four-arm spiral arm model (left) introduced in (4) and the axisymmetric base model (right).

These spiral-arm tangents are seen as the local enhancements of gamma-ray flux in the Galactic plane. At these energies, however, gamma-ray emission predominantly stems from the decay of neutral pions formed in nuclear reactions between cosmic-ray nuclei and the interstellar gas. Correspondingly, these enhancements are not directly visible in the total gamma-ray flux, partly because of the dominant structure by the interstellar gas acting as the target for the pion-

decay and also the bremsstrahlung channel. They can, however, be quantified by comparing the gamma-ray spectra for the two models as shown in Fig. 3. Apparently, results between the axisymmetric model and the model using a spiral-arm source distribution are very similar at the chosen off-arm position, whereas there is a clear enhancement of the cosmic-ray flux at the position of the Norma spiral-arm tangent.

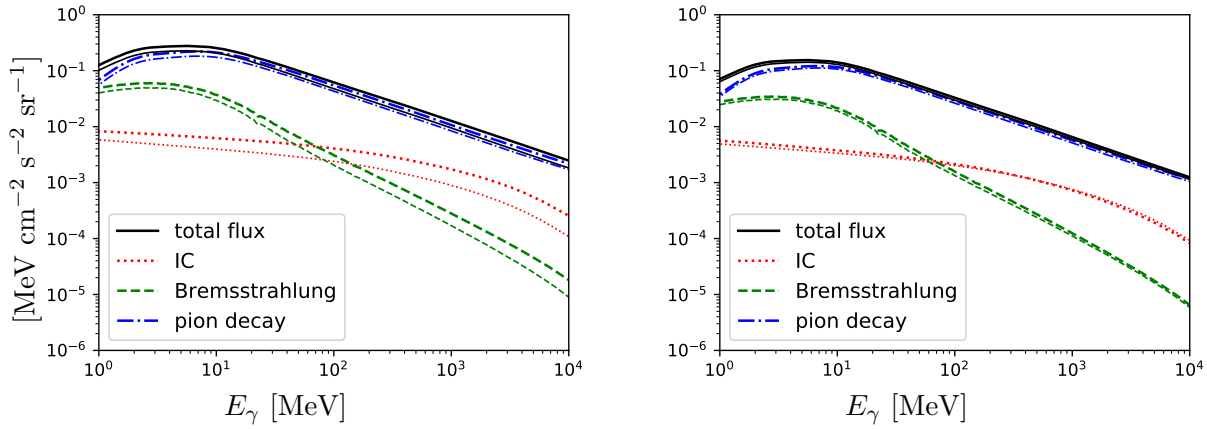

Figure 3. Spectra for the different gamma-ray emission channels (as indicated in the legend) in the direction of a spiral-arm tangent (left) and in the direction without a spiral arm (right). Data are shown for the Norma arm at a Galactic longitude of -30° and at a longitude of -35° for the off-arm position. For each channel we compare our results for the spiral-arm source distribution model with such for the axisymmetric model, where the results for the latter is given by the thinner lines.

At this point one has to keep in mind that the spiral-arm structure of our Galaxy does not only affect the distribution of the cosmic-ray sources. Where other authors investigated the related impact of the gas distribution or the interstellar radiation field (1; 6), we also considered the impact of the interstellar magnetic field that according to observations is aligned with the Galactic spiral arms (37; 38). Here, we do not discuss the related synchrotron emission, but rather apply the theoretical prediction that diffusion differs fundamentally along and perpendicular to the background magnetic field (12). We modeled a case where diffusion along the magnetic field is one order of magnitude stronger than in the perpendicular direction as also discussed in (2). For this we used an analytical magnetic-field configuration from (37). Specifically, we implemented their model Dd for the field, which features magnetic field lines along the spiral arms in the Galactic plane and an X-shape magnetic field structure in the Galactic halo.

As a consequence of this model the diffusion of cosmic rays perpendicular to the spiral arms becomes weaker than in the isotropic diffusion case and, thus, the contrast between on-arm and inter-arm regions is enhanced. This also has an impact on gamma-ray emission, where local enhancements also become visible in the total gamma-ray flux. This is shown in Fig. 4, where we compare results for the case with isotropic and with anisotropic diffusion for the four-arm spiral arm source model. Both models use a transport-parameter set that leads to cosmic-ray fluxes at Earth that are compatible with local measurements.

One of the first studies going beyond analytically prescribed source distributions (1) was motivated by the finding that most axismmetric cosmic-ray source distributions peak around a Galactocentric radius of 4 kpc, while strongly decreasing towards the Galactic center. The latter is in contrast, e.g., to the observed star-formation rate or estimates of the rate of supernova

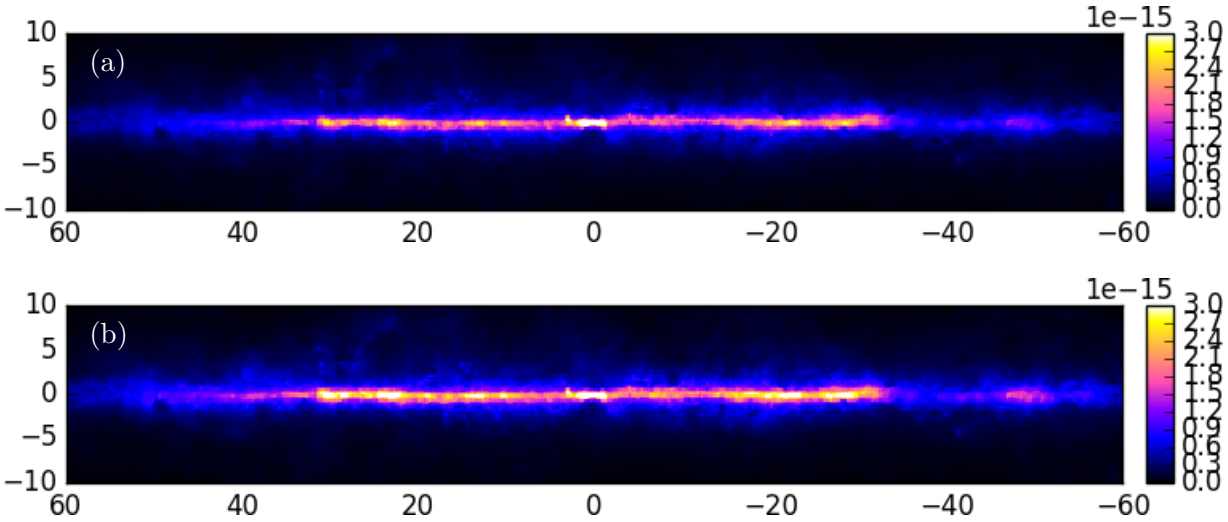

Figure 4. Impact of anisotropic diffusion on the total gamma-ray emission. Here, we compare results for the four-arm spiral arm model with isotropic (a) and anisotropic (b) spatial diffusion. Results are shown for the inner Galaxy at an energy of ∼1 TeV. Gamma-ray emission is given in units of [MeV^{-1} cm^{-2} s^{-2} sr^{-1}].

explosions in the vicinity of the Galactic center (see (1) and references therein). While the impact of the cosmic-ray source distribution near the Galactic center is negligible with regard to the cosmic-ray flux at Earth, it certainly has an important impact on the diffuse gamma-ray emission in the direction of the Galactic center. Therefore, (1) investigated a source model using a component based on tracers of molecular hydrogen, leading to a decrease of the intensity of the Galactic center excess (39; 40).

In contrast to tracing the cosmic-ray sources by the distribution of H_2, linked to the Galactic star-formation regions, especially observations of very-high-energy gamma-rays in the Galactic plane (see, e.g., (41)) show the most energetic gamma-ray sources, which should also be relevant sources of the highest-energetic Galactic cosmic rays. At least at this energy we obviously have to work with individual sources instead of a smooth distribution. Given that the distance estimates to the individual observed sources are not very accurate, it is hard to determine if the sources indeed predominantly occur within the Galactic spiral arms. (41) find a slight enhancement of the source density in the direction of some spiral-arm tangents, but the small-number statistics in this case does not allow any firm conclusions.

Nonetheless, we used these observations to build a three-dimensional source model for Galactic cosmic-ray transport with a focus on very-high-energy gamma-ray emission. For this we adapted all sources from the H.E.S.S. Galactic plane survey (HGPS) (41), for which at least an estimate on the distance was known, and additionally took the Galactic center source and the Crab nebula into account. To consider those sources that are beyond the sensitivity of the HGPS, we additionally included a range of sources that were statistically distributed throughout the Galaxy, where the related distribution function is motivated from the usual four-arm spiral model of the Galaxy including a Galactic bar (35). For these sources the distribution of the source luminosities was adapted to closely represent related results from the HGPS and also the luminosity distribution in the Galactic plane was adapted to be rather isotropic (42; 43). We also introduced different source types as leptonic, hardronic, or composite sources with fractions taken from the HGPS.

For this source model we also find an azimuthally averaged cosmic-ray source density that actually peaks near the Galactic center (see Fig. 5) similar to the study by (1). This similarity

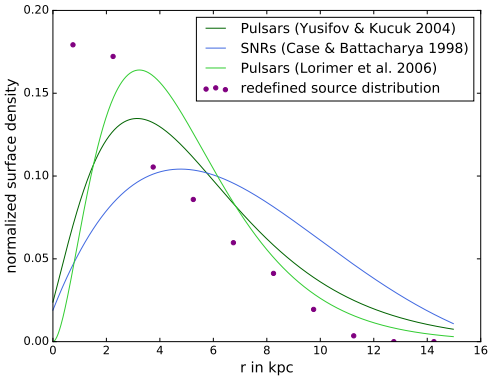

Figure 5. Azimuthally averaged cosmic-ray source density for the new three-dimensional cosmic-ray source distribution (filled circles) as a function of Galactocentric radius in comparison to commonly used axisymmetric source distributions by (44) (dark green) (45) (blue), and (46) (light green). All curves are normalised to yield the same integral source count. Figure taken from (47).

probably relates to the presence of the Galactic bar that is visible in the H_2 distribution used in (1) and that is also included in our statistical source model. Our source model was then implemented in PICARD and the full transport equation solved using an isotropic diffusion model – in this case, it will be particularly interesting to observe the effect of anisotropic diffusion, which we plan to do in the near future. Again, the transport parameters were adapted in a way as to yield a good fit to cosmic-ray spectra observed at Earth (47).

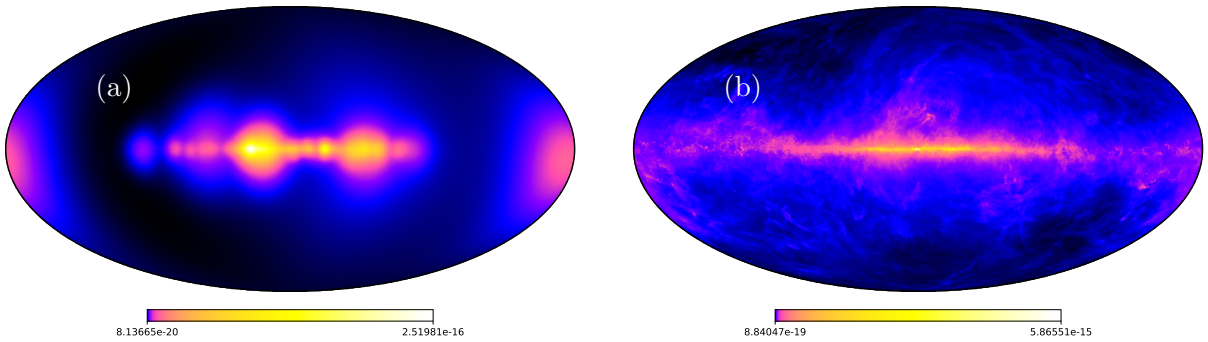

Figure 6. Inverse-Compton (a) and total (b) gamma-ray emission at an energy of ∼1 TeV for the transport model with the three-dimensional cosmic-ray source distribution as described in the text. Gamma-ray emission is given in units of [MeV^{-1} cm^{-2} s^{-2} sr^{-1}].

The propagation results were then used to compute the ensuing gamma-ray emission at an energy of ∼1 TeV shown in Fig. 6. In the inverse Compton channel the imprint of the source localisation becomes obvious, but it also has some impact on the total gamma-ray emission. To avoid problems with the spatial resolution all sources were implemented as a Gaussian with $\sigma = 300$ pc. This value will be decreased in the future possibly leading to less extended structures for the inverse-Compton emission. Nonetheless, these preliminary results show both the capability of the PICARD code to capture three-dimensional geometries in Galactic cosmic-ray transport and that such distributions of individual sources can also leave an imprint on the total gamma-ray emission beyond the one by the distribution of the interstellar gas.

4. Conclusion

Here, we gave an overview of the capabilities, recent developments, and applications of the PICARD code. This code was developed with a focus on numerical efficiency and accuracy especially related to spatially three-dimensional models on Galactic cosmic-ray transport. Here,

we in particular discussed the convergence properties of the code, leading to an estimate of typical magnitudes for the discretisation error. Results briefly discussed here relate to different realisations of three-dimensional source distributions in Galactic cosmic-ray transport. For these anisotropic diffusion was shown to possibly enhance localised structures to a sufficient degree to become visible in diffuse gamma-ray emission. In this context also a first implementation of a localised source model based on the H.E.S.S. Galactic plane survey indicates that part of the structuring in Galactic diffuse gamma-ray emission, especially at TeV energies, could actually related to source localisation. These latter models will be improved in the future by using an even more accurate source model together with a more realistic source extension and individual source spectra.

References

[1] Carlson E, Linden T and Profumo S 2016 *Phys. Rev. D* **94** 063504 (*Preprint* 1603.06584)

[2] Effenberger F, Fichtner H, Scherer K and Büsching I 2012 *A&A* **547** A120 (*Preprint* 1210.1423)

[3] Jóhannesson G, Porter T A and Moskalenko I V 2018 *ApJ* **856** 45 (*Preprint* 1802.08646)

[4] Kissmann R, Werner M, Reimer O and Strong A W 2015 *Astroparticle Physics* **70** 39–53 (*Preprint* 1504.08249)

[5] Niederwanger F, Reimer O, Kissmann R, Strong A W, Popescu C C and Tuffs R 2019 *Astroparticle Physics* **107** 1–14 (*Preprint* 1811.12683)

[6] Porter T A, Jóhannesson G and Moskalenko I V 2017 *ApJ* **846** 67 (*Preprint* 1708.00816)

[7] Werner M, Kissmann R, Strong A W and Reimer O 2015 *Astroparticle Physics* **64** 18–33 (*Preprint* 1410.5266)

[8] Oliva A, Tomassetti N and Feng J 2017 *35th International Cosmic Ray Conference (ICRC2017)* (*International Cosmic Ray Conference* vol 301) p 270 (*Preprint* 1707.06918)

[9] Tomassetti N 2017 *Phys. Rev. D* **96**(10) 103005 URL https://link.aps.org/doi/10.1103/PhysRevD.96.103005

[10] Berezinskiĭ V and Ginzburg V 1990 *Astrophysics of cosmic rays* (North-Holland) ISBN 9780444886415

[11] Schlickeiser R 2002 *Cosmic Ray Astrophysics* Astronomy and Astrophysics Library (Springer) ISBN 9783540664659

[12] Schlickeiser R 1989 *ApJ* **336** 243–293

[13] Matthaeus W H, Qin G, Bieber J W and Zank G P 2003 *ApJ* **590** L53–L56

[14] Shalchi A, Bieber J W and Matthaeus W H 2004 *ApJ* **615** 805–812

[15] Trotta R, Jóhannesson G, Moskalenko I V, Porter T A, Ruiz de Austri R and Strong A W 2011 *ApJ* **729** 106 (*Preprint* 1011.0037)

[16] Jóhannesson G, Ruiz de Austri R, Vincent A C, Moskalenko I V, Orlando E, Porter T A, Strong A W, Trotta R, Feroz F, Graff P and Hobson M P 2016 *ApJ* **824** 16 (*Preprint* 1602.02243)

[17] Ackermann M, Ajello M, Atwood W B, Baldini L, Ballet J, Barbiellini G, Bastieri D, Bechtol K, Bellazzini R, Berenji B, Blandford R D, Bloom E D, Bonamente E, Borgland A W, Brandt T J, Bregeon J, Brigida M, Bruel P, Buehler R, Buson S, Caliandro G A, Cameron R A, Caraveo P A, Cavazzuti E, Cecchi C, Charles E, Chekhtman A, Chiang J, Ciprini S, Claus R, Cohen-Tanugi J, Conrad J, Cutini S, de Angelis A, de Palma F, Dermer C D, Digel S W, Silva E d C e, Drell P S, Drlica-Wagner A, Falletti L, Favuzzi C, Fegan S J, Ferrara E C, Focke W B, Fortin P, Fukazawa Y, Funk S, Fusco P, Gaggero D, Gargano F, Germani S, Giglietto N, Giordano F, Giroletti M, Glanzman T, Godfrey G,

Grove J E, Guiriec S, Gustafsson M, Hadasch D, Hanabata Y, Harding A K, Hayashida M, Hays E, Horan D, Hou X, Hughes R E, Jóhannesson G, Johnson A S, Johnson R P, Kamae T, Katagiri H, Kataoka J, Knödlseder J, Kuss M, Lande J, Latronico L, Lee S H, Lemoine-Goumard M, Longo F, Loparco F, Lott B, Lovellette M N, Lubrano P, Mazziotta M N, McEnery J E, Michelson P F, Mitthumsiri W, Mizuno T, Monte C, Monzani M E, Morselli A, Moskalenko I V, Murgia S, Naumann-Godo M, Norris J P, Nuss E, Ohsugi T, Okumura A, Omodei N, Orlando E, Ormes J F, Paneque D, Panetta J H, Parent D, Pesce-Rollins M, Pierbattista M, Piron F, Pivato G, Porter T A, Rainò S, Rando R, Razzano M, Razzaque S, Reimer A, Reimer O, Sadrozinski H F W, Sgrò C, Siskind E J, Spandre G, Spinelli P, Strong A W, Suson D J, Takahashi H, Tanaka T, Thayer J G, Thayer J B, Thompson D J, Tibaldo L, Tinivella M, Torres D F, Tosti G, Troja E, Usher T L, Vandenbroucke J, Vasileiou V, Vianello G, Vitale V, Waite A P, Wang P, Winer B L, Wood K S, Wood M, Yang Z, Ziegler M and Zimmer S 2012 *ApJ* **750** 3

[18] Gaggero D, Urbano A, Valli M and Ullio P 2015 *Phys. Rev. D* **91** 083012 (*Preprint* 1411.7623)

[19] Popescu C C, Yang R, Tuffs R J, Natale G, Rushton M and Aharonian F 2017 *MNRAS* **470** 2539–2558 (*Preprint* 1705.06652)

[20] Kissmann R 2014 *Astroparticle Physics* **55** 37–50 (*Preprint* 1401.4035)

[21] Maurin D 2020 *Computer Physics Communications* **247** 106942

[22] Evoli C, Gaggero D, Vittino A, Di Bernardo G, Di Mauro M, Ligorini A, Ullio P and Grasso D 2017 *J. Cosmology Astropart. Phys.* **2017** 015 (*Preprint* 1607.07886)

[23] Moskalenko I V and Strong A W 1998 *ApJ* **493** 694 (*Preprint* astro-ph/9710124)

[24] Strong A W and Moskalenko I V 1998 *ApJ* **509** 212–228 (*Preprint* arXiv:astro-ph/9807150)

[25] Benyamin D, Nakar E, Piran T and Shaviv N J 2014 *ApJ* **782** 34 (*Preprint* 1308.1727)

[26] Kopp A, Büsching I, Strauss R D and Potgieter M S 2012 *Computer Physics Communications* **183** 530–542

[27] Strauss R D T and Effenberger F 2017 *Space Sci. Rev.* **212** 151–192 (*Preprint* 1703.06192)

[28] Merten L, Becker Tjus J, Fichtner H, Eichmann B and Sigl G 2017 *J. Cosmology Astropart. Phys.* **2017** 046 (*Preprint* 1704.07484)

[29] Strong A W, Moskalenko I V and Ptuskin V S 2007 *Annual Review of Nuclear and Particle Science* **57** 285–327 (*Preprint* arXiv:astro-ph/0701517)

[30] Trottenberg U, Osterlee C and Schuller A 2001 *Multigrid* (Orlando, FL, USA: Academic Press, Inc.) ISBN 0-12-701070-X

[31] Trottenberg U, , Ooosterlee C W and Schüller A 2001 *Multigrid* (Orlando, FL, USA: Academic Press, Inc.) ISBN 0-12-701070-X

[32] Ackermann M, Ajello M, Atwood W B, Baldini L, Ballet J, Barbiellini G, Bastieri D, Bechtol K, Bellazzini R, Berenji B, Blandford R D, Bloom E D, Bonamente E, Borgland A W, Brandt T J, Bregeon J, Brigida M, Bruel P, Buehler R, Buson S, Caliandro G A, Cameron R A, Caraveo P A, Cavazzuti E, Cecchi C, Charles E, Chekhtman A, Chiang J, Ciprini S, Claus R, Cohen-Tanugi J, Conrad J, Cutini S, de Angelis A, de Palma F, Dermer C D, Digel S W, Silva E d C e, Drell P S, Drlica-Wagner A, Falletti L, Favuzzi C, Fegan S J, Ferrara E C, Focke W B, Fortin P, Fukazawa Y, Funk S, Fusco P, Gaggero D, Gargano F, Germani S, Giglietto N, Giordano F, Giroletti M, Glanzman T, Godfrey G, Grove J E, Guiriec S, Gustafsson M, Hadasch D, Hanabata Y, Harding A K, Hayashida M, Hays E, Horan D, Hou X, Hughes R E, Jóhannesson G, Johnson A S, Johnson R P, Kamae

T, Katagiri H, Kataoka J, Knödlseder J, Kuss M, Lande J, Latronico L, Lee S H, Lemoine-Goumard M, Longo F, Loparco F, Lott B, Lovellette M N, Lubrano P, Mazziotta M N, McEnery J E, Michelson P F, Mitthumsiri W, Mizuno T, Monte C, Monzani M E, Morselli A, Moskalenko I V, Murgia S, Naumann-Godo M, Norris J P, Nuss E, Ohsugi T, Okumura A, Omodei N, Orlando E, Ormes J F, Paneque D, Panetta J H, Parent D, Pesce-Rollins M, Pierbattista M, Piron F, Pivato G, Porter T A, Rainò S, Rando R, Razzano M, Razzaque S, Reimer A, Reimer O, Sadrozinski H F W, Sgrò C, Siskind E J, Spandre G, Spinelli P, Strong A W, Suson D J, Takahashi H, Tanaka T, Thayer J G, Thayer J B, Thompson D J, Tibaldo L, Tinivella M, Torres D F, Tosti G, Troja E, Usher T L, Vandenbroucke J, Vasileiou V, Vianello G, Vitale V, Waite A P, Wang P, Winer B L, Wood K S, Wood M, Yang Z, Ziegler M and Zimmer S 2012 *ApJ* **750** 3

[33] Moskalenko I V, Strong A W, Ormes J F and Potgieter M S 2002 *ApJ* **565** 280–296 (*Preprint* `astro-ph/0106567`)

[34] Dundovic A, Evoli C and Gaggero D 2020 HERMES - High-Energy Radiative MESsangers Code `https://github.com/cosmicrays/hermes` [Online; accessed 25-Februar-2020]

[35] Steiman-Cameron T Y, Wolfire M and Hollenbach D 2010 *ApJ* **722** 1460–1473

[36] Kissmann R, Niederwanger F, Reimer O and Strong A W 2017 *6th International Symposium on High Energy Gamma-Ray Astronomy* (*American Institute of Physics Conference Series* vol 1792) p 070011 (*Preprint* `1701.07285`)

[37] Ferrière K and Terral P 2014 *A&A* **561** A100 (*Preprint* `1312.1974`)

[38] Jansson R and Farrar G R 2012 *ApJ* **757** 14 (*Preprint* `1204.3662`)

[39] Daylan T, Finkbeiner D P, Hooper D, Linden T, Portillo S K N, Rodd N L and Slatyer T R 2016 *Physics of the Dark Universe* **12** 1–23 (*Preprint* `1402.6703`)

[40] Calore F, Cholis I and Weniger C 2015 *J. Cosmology Astropart. Phys.* **2015** 038 (*Preprint* `1409.0042`)

[41] H E S S Collaboration, Abdalla H, Abramowski A, Aharonian F, Benkhali F A, Angüner E O, Arakawa M, Arrieta M, Aubert P, Backes M, Balzer A, Barnard M, Becherini Y, Tjus J B, Berge D, Bernhard S, Bernlöhr K, Blackwell R, Böttcher M, Boisson C, Bolmont J, Bonnefoy S, Bordas P, Bregeon J, Brun F, Brun P, Bryan M, Büchele M, Bulik T, Capasso M, Carrigan S, Caroff S, Carosi A, Casanova S, Cerruti M, Chakraborty N, Chaves R C G, Chen A, Chevalier J, Colafrancesco S, Condon B, Conrad J, Davids I D, Decock J, Deil C, Devin J, deWilt P, Dirson L, Djannati-Ataï A, Domainko W, Donath A, Drury L O C, Dutson K, Dyks J, Edwards T, Egberts K, Eger P, Emery G, Ernenwein J P, Eschbach S, Farnier C, Fegan S, Fernandes M V, Fiasson A, Fontaine G, Förster A, Funk S, Füßling M, Gabici S, Gallant Y A, Garrigoux T, Gast H, Gaté F, Giavitto G, Giebels B, Glawion D, Glicenstein J F, Gottschall D, Grondin M H, Hahn J, Haupt M, Hawkes J, Heinzelmann G, Henri G, Hermann G, Hinton J A, Hofmann W, Hoischen C, Holch T L, Holler M, Horns D, Ivascenko A, Iwasaki H, Jacholkowska A, Jamrozy M, Jankowsky D, Jankowsky F, Jingo M, Jouvin L, Jung-Richardt I, Kastendieck M A, Katarzyński K, Katsuragawa M, Katz U, Kerszberg D, Khangulyan D, Khélifi B, King J, Klepser S, Klochkov D, Kluźniak W, Komin N, Kosack K, Krakau S, Kraus M, Krüger P P, Laffon H, Lamanna G, Lau J, Lees J P, Lefaucheur J, Lemière A, Lemoine-Goumard M, Lenain J P, Leser E, Lohse T, Lorentz M, Liu R, López-Coto R, Lypova I, Marandon V, Malyshev D, Marcowith A, Mariaud C, Marx R, Maurin G, Maxted N, Mayer M, Meintjes P J, Meyer M, Mitchell A M W, Moderski R, Mohamed M, Mohrmann L, Morå K, Moulin E, Murach T, Nakashima S, de Naurois M, Ndiyavala H, Niederwanger F, Niemiec J, Oakes L, O'Brien P, Odaka H, Ohm S, Ostrowski M, Oya I, Padovani M, Panter M, Parsons R D, Paz Arribas M, Pekeur N W, Pelletier G, Perennes C, Petrucci P O, Peyaud B, Piel Q, Pita S, Poireau V, Poon

H, Prokhorov D, Prokoph H, Pühlhofer G, Punch M, Quirrenbach A, Raab S, Rauth R, Reimer A, Reimer O, Renaud M, de los Reyes R, Rieger F, Rinchiuso L, Romoli C, Rowell G, Rudak B, Rulten C B, Safi-Harb S, Sahakian V, Saito S, Sanchez D A, Santangelo A, Sasaki M, Schandri M, Schlickeiser R, Schüssler F, Schulz A, Schwanke U, Schwemmer S, Seglar-Arroyo M, Settimo M, Seyffert A S, Shafi N, Shilon I, Shiningayamwe K, Simoni R, Sol H, Spanier F, Spir-Jacob M, Stawarz Ł, Steenkamp R, Stegmann C, Steppa C, Sushch I, Takahashi T, Tavernet J P, Tavernier T, Taylor A M, Terrier R, Tibaldo L, Tiziani D, Tluczykont M, Trichard C, Tsirou M, Tsuji N, Tuffs R, Uchiyama Y, van der Walt D J, van Eldik C, van Rensburg C, van Soelen B, Vasileiadis G, Veh J, Venter C, Viana A, Vincent P, Vink J, Voisin F, Völk H J, Vuillaume T, Wadiasingh Z, Wagner S J, Wagner P, Wagner R M, White R, Wierzcholska A, Willmann P, Wörnlein A, Wouters D, Yang R, Zaborov D, Zacharias M, Zanin R, Zdziarski A A, Zech A, Zefi F, Ziegler A, Zorn J and Żywucka N 2018 *A&A* **612** A1

[42] Egberts K 2017 *35th International Cosmic Ray Conference (ICRC2017)* (*International Cosmic Ray Conference* vol 301) p 684

[43] Steppa C 2019 *36th International Cosmic Ray Conference (ICRC2019)* (*International Cosmic Ray Conference* vol 36) p 801

[44] Yusifov I and Küçük I 2004 *A&A* **422** 545–553 (*Preprint* `astro-ph/0405559`)

[45] Case G L and Bhattacharya D 1998 *ApJ* **504** 761–772 (*Preprint* `astro-ph/9807162`)

[46] Lorimer D R, Faulkner A J, Lyne A G, Manchester R N, Kramer M, McLaughlin M A, Hobbs G, Possenti A, Stairs I H, Camilo F, Burgay M, D'Amico N, Corongiu A and Crawford F 2006 *MNRAS* **372** 777–800 (*Preprint* `astro-ph/0607640`)

[47] Thaler J 2019 *Redefining the cosmic-ray distribution for Galactic propagation* Master's thesis Universität Innsbruck Austria